Wave-function geometry of band crossing points in two dimensions

Yoonseok Hwang, Junseo Jung, Jun-Won Rhim, and Bohm-Jung Yang

Phys. Rev. B **103**, L241102 — Published 8 June 2021

DOI: 10.1103/PhysRevB.103.L241102

Wave function geometry of band crossing points in two-dimensions

Yoonseok Hwang,[1,2,3,*] Junseo Jung,[1,2,*] Jun-Won Rhim,[1,2,4] and Bohm-Jung Yang[1,2,3,†]

[1] *Center for Correlated Electron Systems, Institute for Basic Science (IBS), Seoul 08826, Korea*
[2] *Department of Physics and Astronomy, Seoul National University, Seoul 08826, Korea*
[3] *Center for Theoretical Physics (CTP), Seoul National University, Seoul 08826, Korea*
[4] *Department of Physics, Ajou University, 16499, Suwon, Korea*

Geometry of the wave function is a central pillar of modern solid state physics. In this work, we unveil the wave function geometry of two-dimensional semimetals with band crossing points (BCPs). We show that the Berry phase of BCPs are governed by the quantum metric describing the infinitesimal distance between quantum states. For generic linear BCPs, we show that the corresponding Berry phase is determined either by an angular integral of the quantum metric or, equivalently, by the maximum quantum distance of Bloch states. This naturally explains the origin of the π-Berry phase of a linear BCP. In the case of quadratic BCPs, the Berry phase can take an arbitrary value between 0 and 2π. We find simple relations between the Berry phase, maximum quantum distance, and the quantum metric in two cases: i) when one of the two crossing bands is flat, ii) when the system has rotation and/or time-reversal symmetries. To demonstrate the implication of the continuum model analysis in lattice systems, we study tight-binding Hamiltonians describing quadratic BCPs. We show that, when the Berry curvature is absent, a quadratic BCP with an arbitrary Berry phase always accompanies another quadratic BCP so that the total Berry phase of the periodic system becomes zero. This work demonstrates that the quantum metric plays a critical role in understanding the geometric properties of topological semimetals.

Introduction.— The Berry phase of electronic wave functions can have profound effects on vast physical phenomena in condensed matter [1–4]. The significance of the Berry phase lies in the fact that it is not only gauge-invariant (up to an integer multiple of 2π) but also geometric. For instance, the Berry phase, normally written as a line integral of the Berry connection over a loop in the parameter space, can also be expressed as a surface integral of the Berry curvature so that it can be understood as an Aharonov-Bohm phase arising from the Berry gauge flux. The geometric interpretation of the Berry phase in terms of the Berry curvature answers the origin of anomalous Hall effect [5] and also allows us to include various topological phenomena in the realm of the Berry phase related physics [4].

Interestingly, recent studies of topological phases have shown that the Berry phase can also serve as a topological invariant [6–8]. For instance, in a class of topological semimetals having band crossing nodes, the stability of a nodal point in two-dimensions or a nodal line in three-dimensions is guaranteed by the quantized π-Berry phase defined along a loop enclosing the node in momentum space. However, when applied to such band crossing points (BCPs), the geometric interpretation of the Berry phase in terms of the Berry curvature does not work unless a singular source of Berry curvature is introduced. This is because the presence of a band degeneracy inside the loop, on which the Berry phase is defined, prohibits transforming the line integral for the Berry phase to the surface integral with the Berry curvature. In fact, the quantization of Berry phase requires the Berry curvature to vanish because, otherwise, the Berry phase for a BCP becomes path-dependent. This indicates that the geometric character of the Berry phase describing BCPs should have distinct nature, independent of the Berry curvature.

In this work, we unveil the wave function geometry of BCPs in two-dimensional (2D) crystals. Explicitly, we show that the Berry phase is completely determined by the quantum metric [9–15], which describes the infinitesimal distance between two wave functions in the parameter space. Together with the Berry curvature, the quantum metric constitutes the quantum geometric tensor, which fully characterizes the geometry of quantum states. We first show that the maximum quantum distance between the Bloch states around a linear BCP (LBCP) takes the largest allowed value 1 as determined by an angular integral of the quantum metric along a loop enclosing the LBCP. This characteristic property of LBCPs gives rise to the quantized value π of the Berry phase.

In the case of quadratic BCPs (QBCPs) [16, 17], we show that the path-independent Berry phase can take an arbitrary value depending on the Hamiltonian parameters, which modify the quantum metric distribution. We find simple relations between the geometric quantities characterizing the BCPs such as the Berry phase, quantum metric, and maximum quantum distance, in two cases. One is when one of the two crossing bands is flat [18–24]. The other is when the system has rotation or time-reversal symmetries. In both cases, we find that the Berry phase of a QBCP is determined by an angular integral of the quantum metric along a loop enclosing it, which is proportional to the maximum quantum distance of relevant Bloch states.

To demonstrate the implication of the continuum

* These authors contributed equally.
† bjyang@snu.ac.kr

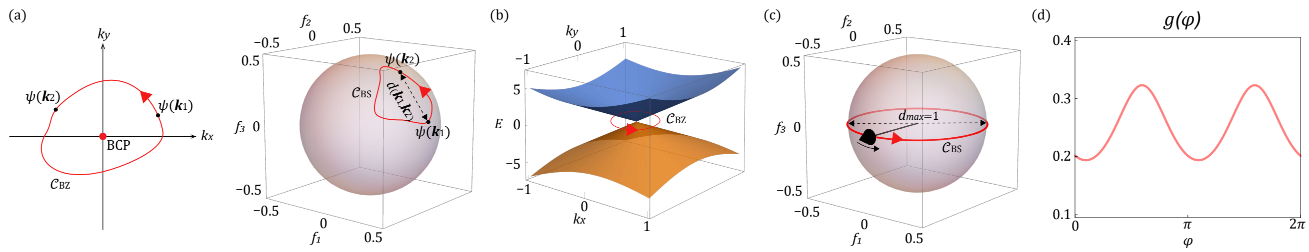

FIG. 1. **Wave function geometry of LBCPs.** (a) Mapping between a closed path $\mathcal{C}_{\rm BZ}$ in momentum space (left) and the loop $\mathcal{C}_{\rm BS}$ on the Bloch sphere $S^2_{\rm BS}$ (right). The straight-line distance between $\check{\boldsymbol{n}}(\boldsymbol{k}_{1,2})$ determines the quantum distance $d(\boldsymbol{k}_1,\boldsymbol{k}_2)$ between $|\psi(\boldsymbol{k}_{1,2})\rangle$. (b) The band structure around an LBCP at $\boldsymbol{k}=(0,0)$ obtained by $H_{\rm L}(\boldsymbol{k})$ with $(t_1,t_2,t_3,b_1,b_2)=(3.9,0.25,-3.5,0,0)$. (c) $\mathcal{C}_{\rm BS}$ on $S^2_{\rm BS}$ corresponding to $\mathcal{C}_{\rm BZ}$ in (b). For an LBCP, the relevant $\mathcal{C}_{\rm BS}$ always forms a great circle, thus the maximum quantum distance is always $d_{\rm max}=1$. The red arrows on $\mathcal{C}_{\rm BZ}$ and $\mathcal{C}_{\rm BS}$ denote their orientation. The big black arrow denotes $\check{\boldsymbol{n}}(0,0)$ which moves counter-clockwisely as the momentum changes along $\mathcal{C}_{\rm BZ}$. (d) Quantum metric $g(\phi)$ in the polar coordinates. While the Berry curvature vanishes everywhere (except at the BCP), the quantum metric is generally non-zero. The integral $\oint d\phi\sqrt{g(\phi)}=\pi d_{\rm max}$ gives the quantized Berry phase $\Phi_B(\mathcal{C}_{\rm BZ})=\pi$ and $d_{\rm max}=1$.

model analysis for the periodic lattice systems, we study tight-binding models describing QBCPs. In the case with vanishing Berry curvature over the whole Brillouin zone (BZ), we find that a QBCP with an arbitrary value of Berry phase always accompanies another BCP. On the other hand, when the Berry curvature is finite, we show that a single QBCP with an arbitrary Berry phase can exist in the BZ. In both lattice models, the obtained geometric quantities of QBCPs are consistent with our continuum theory.

π-Berry phase of LBCPs.— The quantized π-Berry phase of an LBCP (or a Dirac point) [6, 25, 26] has been understood as follows. For a given LBCP, its Berry phase is determined by the line integral of the Berry connection along a loop ℓ enclosing it in momentum space. According to Stokes theorem, the difference of the Berry phases computed along two different loops ℓ_1, ℓ_2 enclosing the LBCP is given by the integral of the Berry curvature over the area S_{ℓ_1,ℓ_2} bounded by ℓ_1, ℓ_2. Then the Berry phase can be path-independent only when the Berry curvature integral over S_{ℓ_1,ℓ_2} vanishes for any choice of ℓ_1, ℓ_2.

Normally, the Berry curvature integral vanishes when suitable symmetry exists such as space-time inversion [27, 28] or mirror symmetries [27] (see Supplemental Materials [29]). Below we show that the Berry phase quantization of LBCPs does not rely on the symmetry but originates from the peculiar geometry of Dirac spinors. The main role of symmetry is to forbid mass terms so that symmetry-protected LBCPs can form a stable Dirac semimetal phase. Even an unstable LBCP appearing at the critical point between insulators has π-Berry phase.

Quantum distance and quantum metric.— To describe the quantum geometry of BCPs, we define several geometric concepts. The Hilbert-Schmidt quantum distance [9, 30–32] between two states $|\psi(\boldsymbol{k})\rangle$ and $|\psi(\boldsymbol{k}')\rangle$ is defined as

$$d^2(\boldsymbol{k},\boldsymbol{k}')=1-|\langle\psi(\boldsymbol{k})|\psi(\boldsymbol{k}')\rangle|^2, \tag{1}$$

which takes the maximal value 1 (minimal value 0) for two orthogonal (identical) states. For two infinitesimally close states at the momentum $\boldsymbol{k}$ and $\boldsymbol{k}'=\boldsymbol{k}+d\boldsymbol{k}$, respectively,

$$d^2(\boldsymbol{k},\boldsymbol{k}+d\boldsymbol{k})=\mathfrak{G}_{ij}(\boldsymbol{k})dk_idk_j, \tag{2}$$

where the quantum geometric tensor $\mathfrak{G}_{ij}(\boldsymbol{k})$, which is hermitian and gauge-invariant, is given by

$$\mathfrak{G}_{ij}(\boldsymbol{k})=\langle\partial_i\psi(\boldsymbol{k})|\partial_j\psi(\boldsymbol{k})\rangle-A_i(\boldsymbol{k})A_j(\boldsymbol{k}), \tag{3}$$

in which $A_i(\boldsymbol{k})=i\langle\psi(\boldsymbol{k})|\partial_i\psi(\boldsymbol{k})\rangle$ indicates the Berry connection. The real and imaginary parts of $\mathfrak{G}_{ij}(\boldsymbol{k})$ correspond to the quantum metric $g_{ij}(\boldsymbol{k})$ and the Berry curvature $F_{ij}(\boldsymbol{k})$, respectively.

Two-band Hamiltonian and Bloch sphere.— In general, BCPs between two non-degenerate bands can be described by a two-band Hamiltonian

$$H(\boldsymbol{k})=f_0(\boldsymbol{k})\sigma_0-\boldsymbol{f}(\boldsymbol{k})\cdot\boldsymbol{\sigma}, \tag{4}$$

where $\boldsymbol{\sigma}=(\sigma_1,\sigma_2,\sigma_3)$ denote the Pauli matrices, σ_0 indicates a 2×2 identity matrix, and $(f_0(\boldsymbol{k}),\boldsymbol{f}(\boldsymbol{k}))=(f_0(\boldsymbol{k}),f_1(\boldsymbol{k}),f_2(\boldsymbol{k}),f_3(\boldsymbol{k}))$ are real functions of $\boldsymbol{k}$. The occupied state $|\psi(\boldsymbol{k})\rangle$ satisfies

$$(\check{\boldsymbol{n}}(\boldsymbol{k})\cdot\boldsymbol{\sigma})|\psi(\boldsymbol{k})\rangle=\frac{1}{2}|\psi(\boldsymbol{k})\rangle, \tag{5}$$

and the corresponding energy eigenvalue is $f_0(\boldsymbol{k})-|\boldsymbol{f}(\boldsymbol{k})|$. Here, $\check{\boldsymbol{n}}(\boldsymbol{k})$ denotes a point on the Bloch sphere $S^2_{\rm BS}$ with radius $r_{\rm BS}=\frac{1}{2}$ defined by

$$\check{\boldsymbol{n}}(\boldsymbol{k})=\frac{1}{2}\frac{\boldsymbol{f}(\boldsymbol{k})}{|\boldsymbol{f}(\boldsymbol{k})|}\in S^2_{\rm BS}. \tag{6}$$

From Eq. (6), one can find several important relations between $|\psi(\boldsymbol{k})\rangle$ in the Hilbert space and $\check{\boldsymbol{n}}(\boldsymbol{k})$ on $S^2_{\rm BS}$ [29]. For this, let us consider a closed path $\mathcal{C}_{\rm BZ}$ enclosing the BCP in momentum space. Then another closed path $C_{\rm BS}$ on $S^2_{\rm BS}$ corresponding to $\mathcal{C}_{\rm BZ}$ is determined by Eq. (6) [see

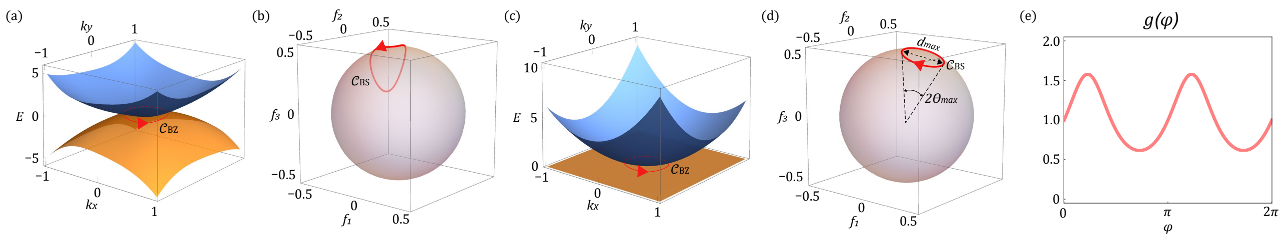

FIG. 2. **Wave function geometry of QBCPs.** (a)-(b) The band structure and the relevant Bloch sphere around a QBCP at $\boldsymbol{k} = (0,0)$ obtained from $H_{\rm Q}(\boldsymbol{k})$ with $(t_1,t_2,t_3,t_4,t_5,t_6,b_1,b_2,b_3) = (-3.8,-0.25,-0.35,1.8,-1.8,2.2,0,0,0)$. $\mathcal{C}_{\rm BS}$ generally has an elliptical shape. (c)-(e) The band structure, the Bloch sphere, and the quantum metric of a QBCP when one of the two crossing bands is flat, obtained from $H_{\rm flat}(\boldsymbol{k})$ with $(t_1,t_2,t_3,t_4,t_5,t_6,b_1,b_2,b_3) = (-1.9,0.9,-1.65,-1.2,0.2842,-1.146,1.9,-0.9,2.029)$. $\mathcal{C}_{\rm BS}$ (red) is a circle with a diameter $d_{\rm max} \in [0,1]$. $2\theta_{\rm max}$ denotes the apex angle for the solid angle subtended by $\mathcal{C}_{\rm BS}$. The apex angle is determined by $d_{\rm max}$: $\cos^2\theta_{\rm max} = 1 - d_{\rm max}^2$. $\oint d\phi\sqrt{g(\phi)} = 2\pi d_{\rm max}$, which is twice larger than the case of the LBCP.

Fig. 1(a)]. First, the quantum distance between $|\psi(\boldsymbol{k}_1)\rangle$ and $|\psi(\boldsymbol{k}_2)\rangle$ is equal to the straight-line distance between $\check{\boldsymbol{n}}(\boldsymbol{k}_1)$ and $\check{\boldsymbol{n}}(\boldsymbol{k}_2)$ on $S^2_{\rm BS}$

$$d(\boldsymbol{k}_1,\boldsymbol{k}_2) = |\check{\boldsymbol{n}}(\boldsymbol{k}_1) - \check{\boldsymbol{n}}(\boldsymbol{k}_2)|. \tag{7}$$

We define the maximum quantum distance $d_{\rm max}$ as the maximum value of $d(\boldsymbol{k}_1,\boldsymbol{k}_2)$ for $\boldsymbol{k}_{1,2} \in \mathcal{C}_{\rm BZ}$.

Second, the length of $\mathcal{C}_{\rm BS}$ is given by an integration of the quantum metric along $\mathcal{C}_{\rm BZ}$:

$$|\mathcal{C}_{\rm BS}| = \oint_{\mathcal{C}_{\rm BZ}} \sqrt{g_{ij}(\boldsymbol{k})dk_i dk_j}. \tag{8}$$

Third, the Berry phase $\Phi_B(\mathcal{C}_{\rm BZ}) = \oint_{\mathcal{C}_{\rm BZ}} d\boldsymbol{k}\cdot\boldsymbol{A}(\boldsymbol{k})$, defined along $\mathcal{C}_{\rm BZ}$, can also be described geometrically on $S^2_{\rm BS}$. Then, $\Phi_B(\mathcal{C}_{\rm BZ})$ is given by a half of the solid angle $\Omega(\mathcal{C}_{\rm BS})$ on $S^2_{\rm BS}$ as

$$\Phi_B(\mathcal{C}_{\rm BZ}) = -\frac{1}{2}\Omega(\mathcal{C}_{\rm BS}) \pmod{2\pi}. \tag{9}$$

In general, there is no closed-form expression relating the three geometric quantities in Eqs. (7)-(9). However, for LBCPs and QBCPs, we demonstrate below the explicit formulas connecting them under the condition that $C_{\rm BS}$ becomes a circle.

Wave function geometry of LBCPs.— The most general form of the $\boldsymbol{k}$ linear Hamiltonian is

$$H^{(0)}_{\rm L}(\boldsymbol{k}) = (b_1k_x + b_2k_y)\sigma_0 + \sum_{a=1}^{3}(v_{ax}k_x + v_{ay}k_y)\sigma_a, \tag{10}$$

where $b_{1,2}$, v_{ai} ($a = 1,2,3$, $i = x,y$) are constants. In general, $H^{(0)}_{\rm L}(\boldsymbol{k})$ does not have any symmetry. But its Berry curvature vanishes at every $\boldsymbol{k}$ so that the BCP at $\boldsymbol{k} = 0$ has a path-independent Berry phase, either 0 or π, depending on $b_{1,2}$, v_{ai}. Here, the Berry curvature vanishes because every term in $H^{(0)}_{\rm L}(\boldsymbol{k})$ is linear in $\boldsymbol{k}$, i.e., $H^{(0)}_{\rm L}(\boldsymbol{k})$ is a homogeneous-order Hamiltonian of degree 1.

After successive unitary transformations [29], $H^{(0)}_{\rm L}(\boldsymbol{k})$ becomes

$$H_{\rm L}(\boldsymbol{k}) = t_3k_y\sigma_1 + (t_1k_x + t_2k_y)\sigma_2 + (b_1k_x + b_2k_y)\sigma_0. \tag{11}$$

We note that $t_{1,3} \neq 0$, because otherwise, $H^{(0)}_{\rm L}(\boldsymbol{k})$ describes a nodal line, not a single LBCP. Comparing Eq. (11) to Eq. (4), we find $\boldsymbol{f}(\boldsymbol{k}) = (-t_3k_y, -t_1k_x - t_2k_y, 0)$, which forms a plane passing through the origin in the three-dimensional space spanned by $(f_1(\boldsymbol{k}), f_2(\boldsymbol{k}), f_3(\boldsymbol{k}))$ when $\boldsymbol{k}$ is varied. For a closed path $\mathcal{C}_{\rm BZ}$ enclosing the origin [see Fig. 1(b)], the corresponding $\mathcal{C}_{\rm BS}$ forms a great circle on $S^2_{\rm BS}$. In this case, the maximum quantum distance $d_{\rm max}$ becomes 1. Hence, we obtain a nodal point at $\boldsymbol{k} = 0$ with $d_{\rm max} = 1$. The band structure, the Bloch sphere, and the quantum metric of $H_{\rm linear}(\boldsymbol{k})$ are shown in Figs. 1(b-d).

For an LBCP described by $H_{\rm L}(\boldsymbol{k})$, the quantum metric tensor $g_{\phi\phi}(\phi) \equiv g(\phi)$ takes a closed form [29] which is plotted in Fig. 1(d) as a function of $\phi = \tan^{-1}(k_y/k_x)$. As the eigenstates of $H_{\rm L}(\boldsymbol{k})$ are independent of $|\boldsymbol{k}|$, they depend only on ϕ so that the relevant Berry curvature vanishes, which is generally valid for any homogeneous-order Hamiltonian. As the Berry curvature is zero, the quantum metric is the only gauge-invariant geometric tensor. When ϕ changes by 2π along a loop $\mathcal{C}_{\rm BZ}$, $\check{\boldsymbol{n}}(\boldsymbol{k})$ also forms a closed loop $\mathcal{C}_{\rm BS}$ with the length $|\mathcal{C}_{\rm BS}| = \oint d\phi\sqrt{g(\phi)} = \pi$ [see Eq. (8)]. We note that $|\mathcal{C}_{\rm BS}|$ is also given by $\pi d_{\rm max}$ since $\mathcal{C}_{\rm BS}$ is the great circle with diameter $d_{\rm max}$. The relevant Berry phase is $\Phi_B(\mathcal{C}_{\rm BZ}) = \pi$, a half of the solid angle $\Omega(\mathcal{C}_{\rm BS}) = 2\pi$ as noted above [see Fig. 1(c)]. The geometrical property of an LBCP can be summarized as follows:

$$d_{\rm max} = \frac{1}{\pi}\oint d\phi\sqrt{g(\phi)} = 1, \quad \Phi_B(\mathcal{C}_{\rm BZ}) = \pi. \tag{12}$$

QBCPs.— Now we consider QBCPs generally described by the Hamiltonian

$$H_{\rm Q}^{(0)}(\boldsymbol{k})=\sum_{a=0}^{3}\sum_{m=0}^{2}v_{a,m}k_x^m k_y^{2-m}\sigma_a, \tag{13}$$

where $v_{a,m}$ $(a=0,1,2,3,\ m=0,1,2)$ are constants. $H_{\rm Q}^{(0)}(\boldsymbol{k})$ has a QBCP at $\boldsymbol{k}=0$ [Fig. 2(a)] and the Berry curvature around it is always zero as $H_{\rm Q}^{(0)}(\boldsymbol{k})$ is a homogeneous-order Hamiltonian. After successive unitary transformations, $H_{\rm Q}^{(0)}(\boldsymbol{k})$ becomes

$$\begin{aligned}H_{\rm Q}(\boldsymbol{k})&=(b_1k_x^2+b_2k_xk_y+b_3k_y^2)\sigma_0+t_6k_y^2\sigma_x\\&+(t_4k_xk_y+t_5k_y^2)\sigma_y+(t_1k_x^2+t_2k_xk_y+t_3k_y^2)\sigma_z,\end{aligned} \tag{14}$$

where $b_{1,2,3}$ and $t_{1,2,\cdots,6}$ are real constants [20]. Here $\boldsymbol{f}(\boldsymbol{k})$ describes a cone in $(f_1(\boldsymbol{k}),f_2(\boldsymbol{k}),f_3(\boldsymbol{k}))$ space as $\boldsymbol{k}$ is varied. As a result, $\mathcal{C}_{\rm BS}$ is no longer a circle but a closed loop with an elliptical shape [see Fig. 2(b)]. Contrary to LBCPs, there is no simple expression connecting the quantum metric and $d_{\rm max}$ for $H_{\rm Q}(\boldsymbol{k})$ in general. Nevertheless, $\mathcal{C}_{\rm BS}$ becomes a circle with arbitrary radius when C_3 or C_6 symmetry exists or a great circle when time-reversal symmetry is further imposed, depending on the symmetry representation. In such cases, the relevant Hamiltonian can be reduced to the Hamiltonian describing a flat band with a QBCP, by adding a term proportional to the identity matrix with an appropriate coefficient. As this procedure does not change the wave function and its geometry, the relevant geometric properties are also identical to those of the flat band with a QBCP, which is discussed below. More details on the QBCPs with rotation and/or time-reversal symmetries are provided in Supplemental Material [29].

Flat band with a QBCP.— Interestingly, the geometric properties of $H_{\rm Q}(\boldsymbol{k})$ can be fully characterized by the quantum metric, if one of the two crossing bands is flat as in Fig. 2(c). We denote such a flat band Hamiltonian by $H_{\rm flat}(\boldsymbol{k})$. It is worth noting that $\mathcal{C}_{\rm BS}$ corresponding to $H_{\rm flat}(\boldsymbol{k})$ is a circle with diameter $d_{\rm max}$ [29] as shown in Fig. 2(d).

The quantum metric $g(\phi)$ of $H_{\rm flat}(\boldsymbol{k})$ also has a closed form [29] which is plotted in Fig. 2(e). We find $|\mathcal{C}_{\rm BS}|=\oint d\phi\sqrt{g(\phi)}=2\pi d_{\rm max}$. Here the additional multiplication factor 2, compared to Eq. (12), arises from the fact that $H_{\rm flat}(\boldsymbol{k})=H_{\rm flat}(-\boldsymbol{k})$, thus $\check{\boldsymbol{n}}(\boldsymbol{k})$ at ϕ and $\phi+\pi$ are identical. As $\check{\boldsymbol{n}}(\boldsymbol{k})$ winds twice for one cyclic change of ϕ, $\mathcal{C}_{\rm BS}$ is two-fold degenerate.

A straightforward calculation gives

$$d_{\rm max}=\frac{1}{2\pi}\int d\phi\sqrt{g(\phi)}=\frac{|t_4|}{(2t_4^2+4t_1t_3-t_2^2)^{1/2}}, \tag{15}$$

which shows that $d_{\rm max}>0$ $(d_{\rm max}=0)$ when $t_4\neq0$ $(t_4=0)$ [22]. The flat band with $d_{\rm max}>0$ $(d_{\rm max}=0)$ is called a singular (non-singular) flat band [20].

The solid angle subtended by $\mathcal{C}_{\rm BS}$ is $\Omega(\mathcal{C}_{\rm BS})=4s\pi(1-\cos\theta_{\rm max})$ where the apex angle $2\theta_{\rm max}$ satisfies $\cos\theta_{\rm max}=\sqrt{1-d_{\rm max}^2}$, and $s=\mathrm{sign}(\frac{t_1t_6}{t_4})=+1$ (-1) indicates the counter-clockwise (clockwise) orientation of $\mathcal{C}_{\rm BS}$. Note that the apex angle is defined so that $\theta_{\rm max}$ is not greater than $\pi/2$ as shown in Fig. 2(d). Hence, the Berry phase is determined by $d_{\rm max}$ as

$$\Phi_B(\mathcal{C}_{\rm BZ})=2s\pi\sqrt{1-d_{\rm max}^2} \tag{16}$$

modulo 2π. We note that the Berry phase around a QBCP can take any value between 0 and 2π (mod 2π). Although vanishing Berry curvature guarantees path-independent Berry phase, its value depends on the Hamiltonian parameters. Also, the quantum metric or the quantum distance is a more useful geometric quantity than the Berry phase for describing BCPs because the Berry phase cannot distinguish singular BCPs with $d_{\rm max}=1$ and non-singular BCPs with $d_{\rm max}=0$. We note that $d_{\rm max}$ of a QBCP becomes 0 or 1, which indicates that the Berry phase is zero modulo 2π, when space-time inversion symmetry exists [29].

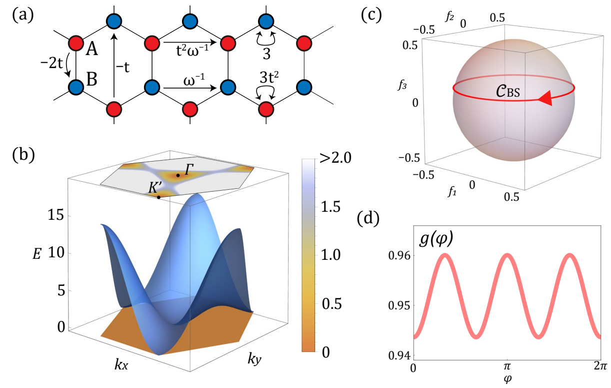

FIG. 3. **A tight-binding model $H_{\rm double}(\boldsymbol{k})$ exhibiting a flat band with two QBCPs.** (a) The honeycomb lattice with two sublattices A and B. Black arrows denote the hopping interactions. Other hopping processes related by C_3 rotation are not shown for clarity. (b) The band structure for $t=0.8$ displaying two QBCPs at Γ and K' points, respectively. The energy difference between two bands is indicated by the intensity plot on the top. (c) The trajectory of the occupied eigenstate on $S^2_{\rm BS}$ as the momentum changes along a circle enclosing the BCP at Γ. A similar circular trajectory with the opposite orientation can be found for the BCP at K'. (d) The quantum metric $g(\phi)$, evaluated along a small circle enclosing the BCP at Γ.

Tight-binding model.— We construct a lattice model displaying our result on a flat band with QBCP. This model is defined on the honeycomb lattice including the hoppings up to third nearest-neighbor sites [Fig. 3(a)]. The lattice Hamiltonian with C_3 symmetry is given by

$$H_{\rm double}(\boldsymbol{k})=\begin{pmatrix}t^2|g(\boldsymbol{k})|^2 & -t\omega^*(g(\boldsymbol{k}))^2\\ -t\omega(g^*(\boldsymbol{k}))^2 & |g(\boldsymbol{k})|^2\end{pmatrix}, \tag{17}$$

where $g(\boldsymbol{k})=e^{-\frac{i}{3}(k_1+k_2)}(1+\omega e^{ik_1}+\omega^{-1}e^{ik_2})$, $(k_1,k_2)=(k_x,\frac{1}{2}k_x+\frac{\sqrt{3}}{2}k_y)$, $\omega=e^{\frac{2\pi i}{3}}$, and t is a real parameter.

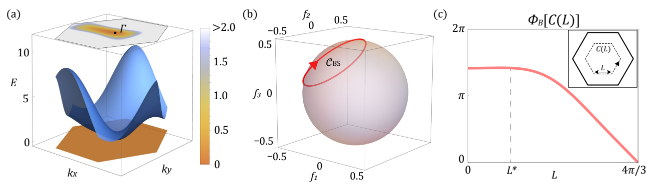

FIG. 4. **A tight-binding model $H_{\rm single}(\boldsymbol{k})$ exhibiting a flat band with a single QBCP.** (a) The band structure of $H_{\rm single}(\boldsymbol{k})$. A flat band has a QBCP at Γ. The energy difference between two bands is indicated by the intensity plot on the top. (b) The trajectory of $|\psi_{\rm flat}(\boldsymbol{k})\rangle$ on $S^2_{\rm BS}$ as the momentum changes along a circle enclosing the BCP at Γ. (c) The Berry phase along the hexagonal closed loop $C(L)$. Near the BCP ($L < L^*$), $\Phi_B[C(L)] \simeq \sqrt{2}\pi$ in accordance with Eq. (16). Because of non-zero Berry curvature, $\Phi_B[C(L)]$ changes as L increases. $C(4\pi/3)$ corresponds to the BZ boundary, and the relevant Berry phase ($\Phi_B[C(4\pi/3)]$) vanishes.

The relevant band structure exhibits two QBCPs at $\Gamma = (0,0)$ and $K' = (\frac{2\pi}{3}, -\frac{2\pi}{\sqrt{3}})$, respectively, [see Fig. 3(b)]. For the QBCP at Γ (K'), we find $\mathcal{C}_{\rm BS}$ with $d_{\rm max} = \frac{2|t|}{t^2+1}$ ($\frac{2|t|}{t^2+1}$) [see Fig. 3(c)], and $\Phi_B = 2\pi\frac{t^2-1}{t^2+1}$ ($-2\pi\frac{t^2-1}{t^2+1}$) satisfying Eq. (16). Hence, the Berry phase can have an arbitrary value depending on t. We note that the model has zero Berry curvature in the BZ except at the BCPs, hence a single BCP at Γ with a nonzero Berry phase must accompany another BCP at K' so that the total Berry phase computed along the BZ boundary becomes 0 (mod 2π).

Meanwhile, a flat band can exhibit a single QBCP with an arbitrary Berry phase when finite Berry curvature exists away from the BCP. To demonstrate this, we construct a lattice model on the honeycomb lattice. Explicitly, the Hamiltonian is given by

$$H_{\rm single}(\boldsymbol{k}) = \frac{1}{4}\begin{pmatrix} |g_2(\boldsymbol{k})|^2 & -g_1(\boldsymbol{k})g_2^*(\boldsymbol{k}) \\ -g_1^*(\boldsymbol{k})g_2(\boldsymbol{k}) & |g_1(\boldsymbol{k})|^2 \end{pmatrix}, \tag{18}$$

where

$$\begin{aligned} g_1(\boldsymbol{k}) &= e^{-\frac{i}{3}(k_1+k_2)}\left(2-(1+i)e^{ik_2}-(1-i)e^{-ik_1+ik_2}\right), \\ g_2(\boldsymbol{k}) &= e^{-\frac{i}{3}(2k_1-k_2)}\left(2-e^{-ik_2}-e^{ik_1-ik_2}\right). \end{aligned} \tag{19}$$

The band structure exhibits a single QBCP at $\Gamma = (0,0)$ with $d_{\rm max} = 1/\sqrt{2}$ [see Figs. 4(a)-(b)]. Since the Berry curvature vanishes only near the BCP, the Berry phase $\Phi_B[C(L)]$, computed along the hexagonal closed loop with edges of length L, is path-independent when the path is close enough to BCP [see Fig. 4(c)]. In accordance with $d_{\rm max} = 1/\sqrt{2}$, $\Phi_B[C(L)]$ converges to $\sqrt{2}\pi$ as $L \to 0$. We note that a single BCP can exist alone as the non-zero Berry curvature makes the Berry phase along the BZ boundary to vanish.

Discussion.— We have focused on BCP(s) in two-band models. However, real materials always contain additional bands whose influence can be understood perturbatively. Namely, starting from the full band structure where two bands form a BCP at $\boldsymbol{k}_0$, the effective Hamiltonian $H_{\rm eff}(\boldsymbol{q})$ for the "crossing bands" near the BCP at $\boldsymbol{k}_0$, where $\boldsymbol{k} = \boldsymbol{k}_0 + \boldsymbol{q}$, can be obtained following the Löwdin perturbation theory [33]. Then the geometric properties of $H_{\rm eff}(\boldsymbol{q})$ can be analyzed using our theory as shown in Supplemental Material [29].

Finally, we note that some lattice models exhibit multi-fold degeneracies where more than two bands cross. For example, recent studies of 3D and 4D multi-fold fermions have shown that the quantum metric is closely related to the Chern number or tensor monopole charge [34–38]. Understanding the quantum geometry of 2D multi-fold degeneracies, using higher-dimensional Bloch spheres, would be an important problem for future study.

ACKNOWLEDGMENTS

Y.H. was supported by IBS-R009-D1 and Samsung Science and Technology Foundation under Project Number SSTF-BA2002-06. J.J. was supported by Basic Science Research Program through the National Research Foundation of Korea (NRF) (Grant No. 0426-20210011) and Samsung Science and Technology Foundation under Project Number SSTF-BA2002-06. J.W.R. was supported by IBS-R009-D1, the National Research Foundation of Korea(NRF) grant funded by the Korea government(MSIT) (Grant No. S-2021-A0403-00170). B.J.Y. was supported by the Institute for Basic Science in Korea (Grant No. IBS-R009-D1), Samsung Science and Technology Foundation under Project Number SSTF-BA2002-06, Basic Science Research Program through the National Research Foundation of Korea (NRF) (Grant No. 0426-20210011), and the U.S. Army Research Office and Asian Office of Aerospace Research & Development (AOARD) under Grant No. W911NF-18-1-0137.

[1] Michael Victor Berry, "Quantal phase factors accompanying adiabatic changes," Proceedings of the Royal Society of London. A. Mathematical and Physical Sciences **392**, 45–57 (1984).
[2] J Zak, "Berrys phase for energy bands in solids," Physical Review Letters **62**, 2747 (1989).
[3] David Vanderbilt and R.D. King-Smith, "Electric polarization as a bulk quantity and its relation to surface charge," Physical Review B **48**, 4442 (1993).
[4] Di Xiao, Ming-Che Chang, and Qian Niu, "Berry phase effects on electronic properties," Reviews of Modern Physics **82**, 1959 (2010).
[5] Nai Phuan Ong and Wei-Li Lee, "Geometry and the anomalous Hall effect in ferromagnets," in *Foundations*

Of Quantum Mechanics In The Light Of New Technology: ISQMTokyo'05 (World Scientific, 2006) pp. 121–126.

[6] M.Z. Hasan and C.L. Kane, "Colloquium: Topological insulators," Reviews of Modern Physics **82**, 3045 (2010).

[7] Xiao-Liang Qi and Shou-Cheng Zhang, "Topological insulators and superconductors," Reviews of Modern Physics **83**, 1057 (2011).

[8] Ching-Kai Chiu, Jeffrey C. Y. Teo, Andreas P. Schnyder, and Shinsei Ryu, "Classification of topological quantum matter with symmetries," Reviews of Modern Physics **88**, 035005 (2016).

[9] JP Provost and G Vallee, "Riemannian structure on manifolds of quantum states," Communications in Mathematical Physics **76**, 289–301 (1980).

[10] Michael V Berry, "The quantum phase, five years after," in *Geometric phases in physics* (World Scientific, Singapore, 1989) pp. 7–28.

[11] J Anandan and Yakir Aharonov, "Geometry of quantum evolution," Physical Review Letters **65**, 1697 (1990).

[12] Paolo Zanardi, Paolo Giorda, and Marco Cozzini, "Information-theoretic differential geometry of quantum phase transitions," Physical Review Letters **99**, 100603 (2007).

[13] Ran Cheng, "Quantum geometric tensor (Fubini-Study metric) in simple quantum system: a pedagogical introduction," arXiv preprint arXiv:1012.1337 (2010).

[14] Raffaele Resta, "The insulating state of matter: a geometrical theory," The European Physical Journal B **79**, 121–137 (2011).

[15] Michael Kolodrubetz, Dries Sels, Pankaj Mehta, and Anatoli Polkovnikov, "Geometry and non-adiabatic response in quantum and classical systems," Physics Reports **697**, 1–87 (2017).

[16] Y.D. Chong, Xiao-Gang Wen, and Marin Soljačić, "Effective theory of quadratic degeneracies," Physical Review B **77**, 235125 (2008).

[17] Kai Sun, Hong Yao, Eduardo Fradkin, and Steven A Kivelson, "Topological insulators and nematic phases from spontaneous symmetry breaking in 2D Fermi systems with a quadratic band crossing," Physical Review Letters **103**, 046811 (2009).

[18] Doron L Bergman, Congjun Wu, and Leon Balents, "Band touching from real-space topology in frustrated hopping models," Physical Review B **78**, 125104 (2008).

[19] Balázs Dóra, Igor F Herbut, and Roderich Moessner, "Occurrence of nematic, topological, and Berry phases when a flat and a parabolic band touch," Physical Review B **90**, 045310 (2014).

[20] Jun-Won Rhim and Bohm-Jung Yang, "Classification of flat bands according to the band-crossing singularity of Bloch wave functions," Physical Review B **99**, 045107 (2019).

[21] Da-Shuai Ma, Yuanfeng Xu, C.S. Chiu, Nicolas Regnault, A.A. Houck, Zhida Song, and B.A. Bernevig, "Spin-orbit-induced topological flat bands in line and split graphs of bipartite lattices," Physical Review Letters **125**, 266403 (2020).

[22] Jun-Won Rhim, Kyoo Kim, and Bohm-Jung Yang, "Quantum distance and anomalous Landau levels of flat bands," Nature **584**, 59–63 (2020).

[23] Jina Ma, Jun-Won Rhim, Liqin Tang, Shiqi Xia, Haiping Wang, Xiuyan Zheng, Shiqiang Xia, Daohong Song, Yi Hu, Yigang Li, *et al.*, "Direct observation of flatband loop states arising from nontrivial real-space topology," Physical Review Letters **124**, 183901 (2020).

[24] Jun-Won Rhim and Bohm-Jung Yang, "Singular flat bands," Advances in Physics: X **6**, 1901606 (2021).

[25] Kostya S Novoselov, Andre K Geim, Sergei Vladimirovich Morozov, Da Jiang, Michail I Katsnelson, IVa Grigorieva, SVb Dubonos, and AA Firsov, "Two-dimensional gas of massless Dirac fermions in graphene," Nature **438**, 197–200 (2005).

[26] Yuanbo Zhang, Yan-Wen Tan, Horst L Stormer, and Philip Kim, "Experimental observation of the quantum Hall effect and Berry's phase in graphene," Nature **438**, 201–204 (2005).

[27] Chen Fang and Liang Fu, "New classes of three-dimensional topological crystalline insulators: Nonsymmorphic and magnetic," Physical Review B **91**, 161105(R) (2015).

[28] Junyeong Ahn and Bohm-Jung Yang, "Unconventional topological phase transition in two-dimensional systems with space-time inversion symmetry," Physical Review Letters **118**, 156401 (2017).

[29] See the Supplemental Material, which includes Refs. [18, 20, 27, 33, 39–41], for more details about the definition and properties of geometric quantities such as the quantum metric, the quantum distance and the Berry phase. The detailed description of tight-binding models and the discussion on multi-band model are also included.

[30] Vladimir Bužek and Mark Hillery, "Quantum copying: Beyond the no-cloning theorem," Physical Review A **54**, 1844 (1996).

[31] C Witte and M Trucks, "A new entanglement measure induced by the Hilbert-Schmidt norm," Physics Letters A **257**, 14–20 (1999).

[32] VV Dodonov, OV Man'Ko, VI Man'Ko, and A Wünsche, "Hilbert-Schmidt distance and non-classicality of states in quantum optics," Journal of Modern Optics **47**, 633–654 (2000).

[33] Per-Olov Löwdin, "A note on the quantum-mechanical perturbation theory," The Journal of Chemical Physics **19**, 1396–1401 (1951).

[34] Giandomenico Palumbo and Nathan Goldman, "Revealing tensor monopoles through quantum-metric measurements," Physical Review Letterss **121**, 170401 (2018).

[35] Grazia Salerno, Nathan Goldman, and Giandomenico Palumbo, "Floquet-engineering of nodal rings and nodal spheres and their characterization using the quantum metric," Physical Review Research **2**, 013224 (2020).

[36] Yu-Ping Lin and Wei-Han Hsiao, "Dual Haldane sphere and quantized band geometry in chiral multifold fermions," Physical Review B **103**, L081103 (2021).

[37] Mo Chen, Changhao Li, Giandomenico Palumbo, Yan-Qing Zhu, Nathan Goldman, and Paola Cappellaro, "A synthetic monopole source of Kalb-Ramond field in diamond," arXiv preprint arXiv:2008.00596 (2020).

[38] Yu-Ping Lin and Wei-Han Hsiao, "Band geometry from position-momentum duality at topological band crossings," arXiv preprint arXiv:2102.04470 (2021).

[39] Bill Sutherland, "Localization of electronic wave functions due to local topology," Physical Review B **34**, 5208 (1986).

[40] Wulayimu Maimaiti, Alexei Andreanov, Hee Chul Park, Oleg Gendelman, and Sergej Flach, "Compact localized states and flat-band generators in one dimension," Physical Review B **95**, 115135 (2017).

[41] N Read, "Compactly supported Wannier functions and

algebraic K-theory," Physical Review B **95**, 115309 (2017).